Cellular/Molecular

Sleep Loss Promotes Astrocytic Phagocytosis and Microglial Activation in Mouse Cerebral Cortex

Michele Bellesi,[1,2] Luisa de Vivo,[1] Mattia Chini,[1] Francesca Gilli,[3] Giulio Tononi,[1] and Chiara Cirelli[1]

[1]Department of Psychiatry, University of Wisconsin–Madison, Madison, Wisconsin 53719, [2]Department of Experimental and Clinical Medicine, Section of Neuroscience and Cell Biology, Università Politecnica delle Marche, Ancona, 60026, Italy, and [3]Department of Neurology, Geisel School of Medicine at Dartmouth, Lebanon, New Hampshire 03756

We previously found that *Mertk* and its ligand *Gas6*, astrocytic genes involved in phagocytosis, are upregulated after acute sleep deprivation. These results suggested that astrocytes may engage in phagocytic activity during extended wake, but direct evidence was lacking. Studies in humans and rodents also found that sleep loss increases peripheral markers of inflammation, but whether these changes are associated with neuroinflammation and/or activation of microglia, the brain's resident innate immune cells, was unknown. Here we used serial block-face scanning electron microscopy to obtain 3D volume measurements of synapses and surrounding astrocytic processes in mouse frontal cortex after 6–8 h of sleep, spontaneous wake, or sleep deprivation (SD) and after chronic (~5 d) sleep restriction (CSR). Astrocytic phagocytosis, mainly of presynaptic components of large synapses, increased after both acute and chronic sleep loss relative to sleep and wake. MERTK expression and lipid peroxidation in synaptoneurosomes also increased to a similar extent after short and long sleep loss, suggesting that astrocytic phagocytosis may represent the brain's response to the increase in synaptic activity associated with prolonged wake, clearing worn components of heavily used synapses. Using confocal microscopy, we then found that CSR but not SD mice show morphological signs of microglial activation and enhanced microglial phagocytosis of synaptic elements, without obvious signs of neuroinflammation in the CSF. Because low-level sustained microglia activation can lead to abnormal responses to a secondary insult, these results suggest that chronic sleep loss, through microglia priming, may predispose the brain to further damage.

Key words: astrocyte; cortex; microglia; mouse; sleep; sleep deprivation

Significance Statement

We find that astrocytic phagocytosis of synaptic elements, mostly of presynaptic origin and in large synapses, is upregulated already after a few hours of sleep deprivation and shows a further significant increase after prolonged and severe sleep loss, suggesting that it may promote the housekeeping of heavily used and strong synapses in response to the increased neuronal activity of extended wake. By contrast, chronic sleep restriction but not acute sleep loss activates microglia, promotes their phagocytic activity, and does so in the absence of overt signs of neuroinflammation, suggesting that like many other stressors, extended sleep disruption may lead to a state of sustained microglia activation, perhaps increasing the brain's susceptibility to other forms of damage.

Introduction

Astrocytes are influenced by changes in behavioral state. Using serial block-face scanning electron microscopy (SBEM), we recently found that most excitatory synapses in mouse frontal cortex are contacted by peripheral astrocytic processes (PAPs). PAPs move closer to the synaptic cleft and expand after extended wake, presumably because the need to clear glutamate and potassium ions increases. Transcriptomic profiling also showed that the expression of ~1.4% of astrocytic genes is state dependent and mostly upregulated in wake relative to sleep (Bellesi et al., 2015). Astrocytic "wake" genes in mice included *Mertk* (Bellesi et al., 2015), and previous experiments in rats found that *Gas6* was upregulated in cortex after chronic sleep deprivation (Cirelli et

Received Dec. 31, 2016; revised March 23, 2017; accepted April 13, 2017.

Author contributions: M.B., G.T., and C.C. designed research; M.B., L.d.V., and M.C. performed research; M.B., L.d.V., M.C., and F.G. analyzed data; M.B., G.T., and C.C. wrote the paper.

This work was supported by NIH Grants DP 1OD579 (G.T.), 1R01MH091326 (G.T.), 1R01MH099231 (G.T., C.C.), and 1P01NS083514 (G.T., C.C.). We thank Benjamin Jones, Hirotaka Nagai, Midori Nagai, Sakiko Honjoh, Alex Rodriguez, Kayla Peelman, Douglas Haswell, and Giovanna Spano for helping with the chronic sleep restriction experiments and Sophia Loschky, Andrea Schroeder, and Samuel Koebe for contributions to EM image analysis.

The authors declare no competing financial interests.

Correspondence should be addressed to Chiara Cirelli, Department of Psychiatry, University of Wisconsin–Madison, 6001 Research Park Boulevard, Madison, WI 53719. E-mail: ccirelli@wisc.edu.

DOI:10.1523/JNEUROSCI.3981-16.2017

 0270-6474/17/375263-11$15.00/0

al., 2006). The receptor MERTK belongs to one of the two pathways that mediate astrocytic phagocytosis (AP; Chung et al., 2015) and through the action of GAS6 (growth arrest-specific protein 6) binds exposed phosphatidylserine in target debris (Grommes et al., 2008). AP participates in developmental synaptic pruning (Berbel and Innocenti, 1988; Chung et al., 2013) and adult astrocytes engulf axonal organelles and synaptic elements even in healthy mice, suggesting that their constitutive phagocytic activity contributes to the clearing of damaged cellular components (Nguyen et al., 2011; Chung et al., 2013; Davis et al., 2014), likely in response to wake-related neuronal activity (Chung et al., 2015).

Microglia are the resident phagocytes of the CNS. They constantly monitor the surrounding microenvironment via their processes, sense neuronal activity, clear neuronal debris after injury and cell death (Wake et al., 2009; Tremblay et al., 2010; Tay et al., 2017), and contribute to developmental synaptic pruning in the healthy brain (Paolicelli et al., 2011; Schafer et al., 2012; Bialas and Stevens, 2013; Sipe et al., 2016). Microglial phagocytosis is mediated by C1q and C3, components of the complement cascade that tag unwanted synapses; by the phagocytic complement receptor expressed by microglia (Stevens et al., 2007); and by MERTK, which is also expressed in microglia (Chung et al., 2013). Any disturbance of brain homeostasis, including inflammation, activates microglia. Acute and chronic sleep deprivation can lead to a pro-inflammatory state in the absence of overt infection or injury (Mullington et al., 2010; Hurtado-Alvarado et al., 2013). Specifically, in humans and rodents, sleep loss can lead to elevated white blood cell counts; increased circulating levels of C-reactive protein, IL1β, IL6, and TNFα (Everson, 2005; Mullington et al., 2010; Hurtado-Alvarado et al., 2013; He et al., 2014); and enhanced permeability of the blood–brain barrier (Hurtado-Alvarado et al., 2013; He et al., 2014). The source of the increase in peripheral cytokines remains unclear but has been linked to the increase in catecholamine levels associated with prolonged wake (Mullington et al., 2010). Equally unclear is whether these peripheral changes are associated with signs of neuroinflammation and/or with microglial activation.

Together, these findings suggest that sleep loss can trigger AP and lead to microglia activation. Here we tested this hypothesis using SBEM to study PAPs surrounding cortical mouse synapses and measured AP occurrence after sleep, spontaneous wake, and sleep loss. In cortical synaptoneurosomes, we also assessed changes in MERTK protein levels and the extent of lipid peroxidation, which can result from high oxidative stress and in turn can trigger phagocytosis. In addition, we measured microglia state of activation and phagocytic activity, as well as levels of inflammatory markers in the CSF of mice after sleep and sleep loss. We find that AP, mainly of presynaptic elements in large synapses, occurs after both acute and chronic sleep loss but not after spontaneous wake, suggesting that it may promote the housekeeping and recycling of worn components of heavily used, strong synapses. By contrast, only chronic sleep loss activates microglia cells and promotes their phagocytic activity, apparently without overt signs of neuroinflammation, suggesting that extended sleep disruption may prime microglia and perhaps predispose the brain to other forms of insult.

Materials and Methods

Animals

Four-week-old homozygous B6.Cg-Tg(Thy1-YFP)16Jrs/J transgenic mice of either sex were used in this study with the exception of microglia experiments, in which 4-week-old male C57BL/6J mice were used. Mice were housed in recording boxes for the duration of the experiment (12 h light/dark cycle, light on at 8:00 A.M., 23 ± 1°C; food and water available *ad libitum* and replaced daily at 8:00 A.M.). All animal procedures followed the National Institutes of Health *Guide for the Care and Use of Laboratory Animals*, and facilities were reviewed and approved by the Institutional Animal Care and Use Committee of the University of Wisconsin–Madison and were inspected and accredited by the Association for Assessment and Accreditation of Laboratory Animal Care.

Experimental conditions and protocols for sleep, spontaneous wake, and acute and chronic sleep loss

Four experimental conditions were used (Fig. 1*A*): (1) sleeping (S) mice were killed during the light phase, at the end of a long period of sleep (>45 min, interrupted by periods of wake of <4 min), and after spending at least 75% of the previous 6–7 h asleep; (2) spontaneously awake (W) mice were killed during the dark phase, at the end of a long period of wake (~1 h, interrupted by periods of sleep of <5 min), and after spending at least 70% of the previous 6–7 h awake; (3) acutely sleep-deprived (SD) mice were killed during the light phase after 8 h of sleep deprivation enforced by introducing novel objects and by tapping on the cage whenever the animals appeared drowsy. As demonstrated in previous studies with EEG recordings, this method can prevent sleep almost completely for several hours [>95% total time spent awake (Cirelli et al., 2004; Bellesi et al., 2013, 2015)]; and (4) chronically sleep-restricted (CSR) mice were subjected in groups (six to eight mice per group) to 4.5 days of chronic sleep restriction using a protocol optimized in our laboratory. A previous validation study that used mice implanted with EEG electrodes found that this CSR protocol results in a reduction of overall sleep duration by ~70% (de Vivo et al., 2016). During chronic sleep restriction, mice were housed in large cages where, during the day, sleep restriction was enforced using ecologically relevant stimuli that included continuous exposure to novel objects, changes of cage and bedding, social interaction, and free access to multiple running wheels. Mild forced locomotion on a slowly rotating platform was used to restrict sleep at night. The platform was located above a tray filled with 2–3 cm of water, and the rotation speed was low enough that mice (still in groups) could easily avoid falling into the water if they moved continuously. Heat lamps were placed ~2 m above the platform to keep mice at the proper temperature. Video cameras and/or direct visual observation were used to continuously monitor the mice. If a mouse fell in the water often enough such that it did not have a chance to dry, it was removed to a cage filled with novel objects and allowed to dry before being placed back onto the rotating platform. Because CSR mice were in groups, sleep and wake could not be quantified with video recording as in S and W mice (see below).

Experimental procedure

S, W, and SD mice were individually housed starting at postnatal day 27 (P27) and killed at P30, and all of them were exposed to a few novel objects and had access to running wheels during the dark phase. CSR mice were subjected to sleep restriction in groups (six to eight mice per group) from P25 to P30. S, SD, and CSR mice were killed at the same time of day (~4:00 P.M.), whereas W mice were killed at ~4:00 A.M. (Fig. 1*A*). Independent groups of S, SD, and CSR mice were used for ultrastructural, molecular, and histological studies (W mice were used only for the ultrastructural studies).

Video recordings of behavioral states. To avoid possible tissue damage and inflammation resulting from the implant of EEG electrodes, behavioral states in S and W mice were determined by continuous video monitoring with infrared cameras. As described previously (Maret et al., 2011; Bellesi et al., 2015), this method consistently estimates total sleep time with ≥90% accuracy even if it cannot distinguish nonrapid eye movement sleep from rapid eye movement sleep. Motor activity was then quantified by custom-made video-based motion detection algorithms (Bellesi et al., 2012).

Ultrastructural studies. The image dataset used for the ultrastructural analysis of astrocytic endocytosis is the same used in a previous study that characterized the dynamics of peripheral astrocytic processes (PAPs) in S, W, SD, and CSR mice (Bellesi et al., 2015), and a detailed description of the methods (perfusion, staining, acquisition, and profiles segmentation) is reported there. Briefly, mice (three animals per group) were perfused

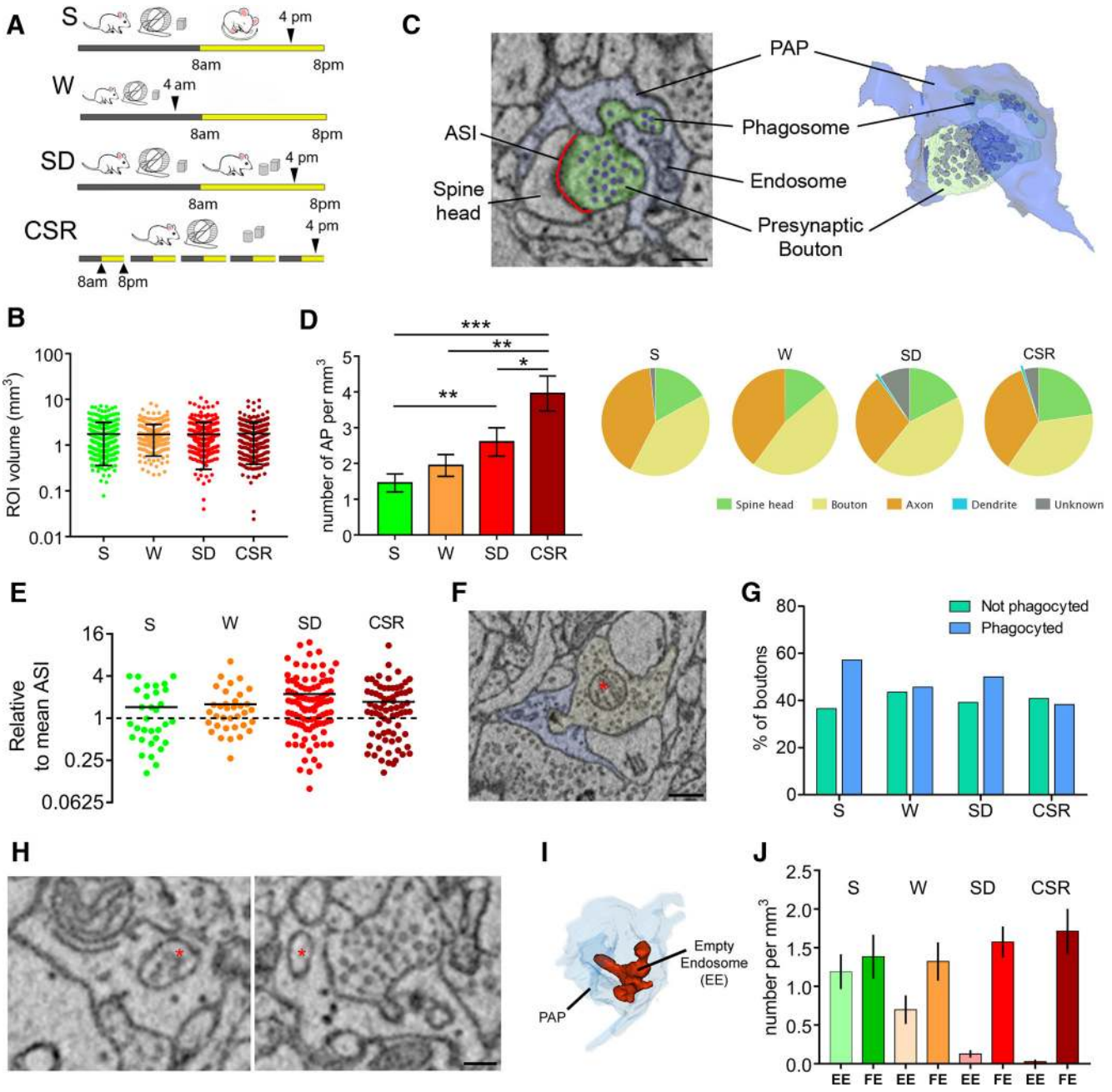

Figure 1. Sleep loss promotes AP. ***A***, Experimental design. ***B***, Volume of all ROIs analyzed in S ($n = 295$), W ($n = 266$), SD ($n = 355$), and CSR ($n = 280$) mice. Black bars depict mean and SD. ***C***, Example of AP as visualized in two-dimensional SBEM images (left) and its 3D reconstruction (right). Scale bar: 200 nm. ***D***, Left, Number of synaptic elements phagocyted by astrocytes in S, W, SD, and CSR mice. Values (mean ± SEM) are expressed per cubed millimeter of astrocytic volume. $^{*}p < 0.05$; $^{**}p < 0.01$; $^{***}p < 0.001$. Right, Breakdown frequency analysis of the neuropil structures involved in AP for S, W, SD, and CSR. ***E***, ASI size of all S, W, SD, and CSR AP+ synapses relative to mean ASI size (dashed line) in a random sample of synapses (S, $n = 302$; W, $n = 256$; SD, $n = 345$; CSR, $n = 296$). ***F***, Example of a presynaptic bouton (yellow) containing a mitochondrion (asterisk) and being phagocyted by a PAP (blue). Scale bar, 400 nm. ***G***, Percentage of presynaptic boutons containing a mitochondrion that are (blue bars) or are not (green bars) involved in AP in S, W, SD, and CSR mice. ***H***, Examples of FE (asterisk, left) and EE (asterisk, right). Scale bar, 130 nm. ***I***, 3D reconstruction of one EE (red). Note its tubular structure within the PAP (light blue). ***J***, Number of EE and FE (mean ± SEM) per cubed millimeter of astrocytic volume in S, W, SD, and CSR mice.

under deep anesthesia (3% isoflurane). Tissue was stained with a solution of 1.5% potassium ferrocyanide/2% osmium tetroxide, followed by 1% thiocarbonhydrazide, 2% osmium tetroxide, and 1% uranyl acetate at 4°C. The following day, the tissue was stained with a solution of lead aspartate, dehydrated, and embedded with Durcupan resin and ACLAR film. Small squares of tissue (1 mm^2) from frontal cortex (anteroposterior, 1.85 mm; mediolateral, 1.5 mm) were glued on the tip of a metal pin and coated with silver paint to minimize specimen charging during imaging.

Image acquisition. Images were obtained using a ΣIGMA VP field emission scanning electron microscope (Carl Zeiss) equipped with 3View technology (Gatan) and a backscattered electron detector (for SBEM). The series of images were processed and analyzed using TrakEM2, a FIJI plug-in (Schindelin et al., 2012). Segmentation of astrocytic profiles was performed manually by two operators blind to the experimental condition. Small cuboid regions of interest (ROIs; 5–6 μm per side) of neuropil (layers II–III, frontal cortex) were selected. PAPs were recognized based on their distinctive shapes, interdigitating among neuronal profiles and often contacting parts of the synapse, and on the presence of glycogen granules. ROIs did not include large dendrites or somata of neurons, glia, or endothelial cells. For each ROI, astrocytic volume and ROI volume were estimated. The occurrence of AP was established by the presence of a portion of axon, spine head, or dendrite being invaginated by

the surrounding PAP, with a clear continuity between the part being enclosed by the PAP (phagosome) and the neuronal structure. AP was quantified using the following score: 1, phagocytosis of the spine head; 2, phagocytosis of the presynaptic bouton; 3, phagocytosis of the axon (outside the axonal bouton); 4, phagocytosis of the dendritic shaft; 5, phagocytosis of an unknown structure. For those synapses whose axonal bouton or spine head were involved in AP, the axon–spine interface (ASI) was manually segmented and measured [as in the study by Bellesi et al. (2015)]. Inside the PAPs, endosomes showing undigested, partially, or fully digested material were scored as full endosomes (FE), whether or not they were fused with lysosomes, whereas the endosomes with no vesicles were scored as empty endosomes (EE).

Microarray: data analysis

We used the microarray data available at the NCBI Gene Expression Omnibus (GEO) database (GSE60079) to perform gene expression analysis of cerebral cortex samples collected from sleeping (6–7 h of sleep during the light phase), awake (6–7 h of spontaneous wake at night), and forced enriched wake (4 h of sleep deprivation through exposure to novel objects during the light phase) mice. Detailed methods were described by Bellesi et al. (2015). Briefly, samples (six for each behavioral state) were collected using the genetically targeted translating ribosome affinity purification methodology from bacterial artificial chromosome transgenic mice expressing EGFP-tagged ribosomal protein L10a in astrocytes. Samples were immunoprecipitated to isolate astrocytes. The precipitated portion formed the bound (IP) sample containing astrocytes, and the remaining part formed the unbound (UB) sample containing all the remaining cell types (neurons and other glia cells). Then, both IP and UB samples were processed, and RNA was extracted and run on Affymetrix GeneChip Mouse Genome 430 2.0 arrays. In the present study, we used array data obtained from the IP samples, and we compared S versus W and S versus SD mice. Data were normalized within each behavioral state group using Robust Multiarray Average. Comparisons were performed using Welch's t test with Benjamini and Hochberg FDR multiple-test correction. All probe sets with fold change >30% and $p < 0.01$ were considered as differentially expressed.

Synaptoneurosome preparation and Western blotting. Under anesthesia, mice (four S, four SD, four CSR) were decapitated, and the cerebral cortex (including the striatum) was quickly collected. Samples were homogenized in ice-cold homogenization buffer [10 mM HEPES (Sigma), 1.0 mM EDTA (Promega), 2.0 mM EGTA (Thermo Fisher Scientific), 0.5 mM DTT (Invitrogen), 0.1 mM PMSF (Fluka), 10 mg/L leupeptin (Sigma), 50 mg/L soybean trypsin inhibitor (Roche), and 100 nM microcystin (Alexis)] using a glass/glass tissue homogenizer (Kontes). A fraction (~10%) of the homogenate from each sample was boiled in 10% SDS for 10 min and stored unprocessed at −80°C. The remaining fraction of the homogenate was passed through two 105 μm pore nylon mesh filters (Small Parts), then through a 5 μm pore filter (Millipore), and centrifuged at 1000 × g for 10 min at 4°C. Pellets were resuspended in 1% SDS, boiled for 10 min, and stored at −80°C. Protein concentration was determined by the bicinchonic acid assay (Pierce). Since housekeeping proteins (e.g., α-actin and β-tubulin) can be affected by sleep and wake, they were not used as an internal standard. Instead, for both homogenates and synaptoneurosomes, equal amounts of protein were pooled from each individual animal within each group. S, SD, and CSR pools (four mice per group) were loaded onto the same gels in three to six replicates (sample loading was randomized). The entire procedure, from pool preparation to sample loading, was repeated four times. In each experiment, equal amounts (5 μg for GFAP, 10 μg for MERTK, 20 μg for C3) of homogenate/synaptoneurosome from S, SD, and CSR pools were separated by Tris-HCl gel electrophoresis (Bio-Rad). Nitrocellulose membranes were probed with anti-GFAP (1:500, Sigma), anti-MERTK (1:500, R&D Systems; AF591), or anti-C3 (1:500, Cappel Laboratories) antibodies. After exposure to secondary antibodies, bands were visualized using enhanced chemiluminescence (ECL-Prime, GE Healthcare) and captured by the Typhoon 9410 Variable Mode Imager (GE Healthcare). Optical densities were calculated for each band of interest after performing background correction (by subtracting the value of a band immediately above the band of interest in the same lane) and normalized within each experiment to the average density of S samples.

Lipid peroxidation. Lipid peroxidation was evaluated in cortical synaptoneurosomes of S ($n = 7$), SD ($n = 8$), and CSR ($n = 7$) mice using the Lipid Peroxidation (MDA) Assay kit (ab118970, Abcam). This assay provides an estimation of the end product [malondialdehyde (MDA)] of lipid peroxidation. Aliquots of synaptoneurosomes (200 μl) were incubated with thiobarbituric acid (TBA) at 95°C for 60 min to generate a MDA–TBA adduct, which was quantified colorimetrically (OD, 532 nm) using a microplate reader.

CSF extraction and Luminex multiplex immune assay. Under anesthesia, S ($n = 11$), SD ($n = 10$), and CSR ($n = 8$) mice were placed on a stereotaxic apparatus, meninges overlying the cisterna magna were exposed, and the surrounding area was gently washed to prevent blood contamination. A small glass capillary tube was used to puncture the arachnoid membrane covering the cisterna magna and collect CSF by capillary action. Approximately 10 μl of CSF were obtained from each mouse and immediately stored at −80°C. Cytokine and chemokine concentrations were measured in a multiplex Luminex assay, i.e., the Bio-Plex Pro Mouse Cytokine 23-plex Assay (Bio-Rad). Individual CSF samples were diluted to 50 μl of volume and incubated with a suspension of analyte capture antibody-conjugated microspheres, per the manufacturer's instructions. After further incubation with biotinylated detection antibodies and phycoerythrin (PE)-conjugated streptavidin, fluorescent signal was read on a Luminex MAGPIX Multiplex Reader (Bio-Rad). A five-parameter logistic curve generated from standards of known concentration was used to convert fluorescent intensity to concentration values, which were then adjusted for sample dilution. The analyzed molecules were IL1a, IL1b, IL2, IL3, IL4, IL5, IL6, IL9, IL10, IL12(p40), IL12(p70), IL13, IL17a, Eotaxin, G-CSF, GM-CSF, IFNγ, KC, MCP1, MIP1a, MIP1b, RANTES, and TNFα.

Immunocytochemistry. S ($n = 6$), SD ($n = 5$), and CSR ($n = 6$) mice were deeply anesthetized with isoflurane (1–1.5% volume) and perfused transcardially with a flush (~30 s) of saline, followed by 4% paraformaldehyde in phosphate buffer. Brains were removed, postfixed in the same fixative overnight, and cut on a vibratome in 50 μm coronal sections. Sections were rinsed in a blocking solution [3% bovine serum albumin (BSA) and 0.3% Triton X-100 for IBA-1 and V-GLUT1, 2% BSA and 0.2% Triton X-100 for MERTK] for 1 h and incubated overnight (4°C) in the same blocking solution containing anti-IBA-1 (1:500, catalog #019-19741, Wako), anti-VGLUT-1 (1:1000, ab5905, Millipore), or anti-MERTK (1:100, AF591, R&D Systems). Sections were then probed with secondary antibodies: Alexa Fluor 568 (1:500, Invitrogen)- and/or Alexa Fluor 488 (1:500, Invitrogen)-conjugated secondary antibodies. For MERTK staining, signal was amplified using anti-goat biotinylated antibodies (1:100, Vector Laboratories) and the TSA kit #22, with HRP–streptavidin and Alexa Fluor 488 Tyramide (T-20932); after the amplification, sections were incubated with anti-GFAP antibodies (1:100, Sigma; overnight at 4°C) and probed with Alexa Fluor 568 (1:500, Invitrogen). Sections were examined with a confocal microscope (Prairie Technologies). For IBA-1, microscopic fields ($n = 5$ per section, 3 sections per mouse) were randomly acquired as 512 × 512 pixel images (pixel size, 581 nm; Z-step, 750 nm) in mouse frontal cortex using a UPlan FL N 40× objective (numerical aperture, 1.3). To improve the signal/noise ratio, two frames of each image were averaged. For IBA-1/VGLUT-1, microscopic fields ($n = 5$ per section, 3 sections per mouse) were randomly acquired as 1024 × 1024 pixel images (pixel size, 65 nm; digital zoom, 3×) in mouse frontal cortex using a UPlan FL N 60× objective (numerical aperture, 1.3).

Image analysis. For IBA-1 staining, all analyses were performed on maximum-intensity projections (Z-project, Maximum Intensity function in ImageJ) of the 28 images constituting the Z-stack. Cell counting was performed manually by two operators blind to the experimental conditions using the cell-counting plugin of FIJI. Two methods were implemented for the morphological analysis of microglia.

Method 1 was adapted from Morrison and Filosa (2013) and consisted on the skeleton analysis of microglial processes. Briefly, background noise of Z-projected images was diminished using the function "Despeckle" in FIJI.

Then, images were binarized, skeletonized, and analyzed using the FIJI plugin "Analyze Skeleton." Branch length and the number of end points (extremities) were then divided by the number of cell somas per frame to obtain normalized values. Method 2 was adapted from Kozlowski and Weimer (2012): images were first thresholded using the "Graythresh" function within MATLAB, and objects with a size comprised between 200 and 1500 pixels, corresponding to putative microglial cells, were identified. To analyze individual cells, the centroid (center of mass) for each of these objects was computed and used to crop an ROI of 110 × 110 pixels around each cell. Each cell mask was visually examined to confirm that a single microglial cell was accurately represented in the mask. Images in which the cell touched the boundary of the image, or images that did not contain a single cell soma, were not considered for further analysis. Overall, 5129 of 8653 microglial cells met the inclusion criteria and were subsequently analyzed using the function "Regionprops" in MATLAB to obtain an estimation of cell perimeter and area. Microglia phagocytosis was quantified in the double-stained IBA-1/VGLUT-1 images. To optimize the detection of the VGLUT-1-positive puncta engulfed within the microglia, green (IBA-1) and red (VGLUT-1) channels were processed separately. The background noise of the green channel was reduced by using the function Subtract Background (rolling ball radius, 50 pixels) in FIJI. The image was subsequently filtered using a 3D hysteresis filter1, followed by a 3D median filter2 in Matlab. The background noise of the red channel was diminished using the function Subtract Background (rolling ball radius, 2 pixels) and Despeckle in FIJI. The image was subsequently filtered through a 3D Maximum Filter (radius, 3 pixels in every dimension), automatically thresholded ("Auto Threshold", "Default" method), and segmented using the "Watershed" function. Green and red channels were then remerged. Only VGLUT-1-positive puncta bigger than 100 pixels (~0.03 μm^3) in *xyz*, and showing 100% overlap with the processed IBA-1 signal, were quantified.

Results

Sleep loss enhances astrocyte phagocytosis

To study the occurrence of astrocytic phagocytosis in the cortical neuropil, tridimensional ROIs were manually segmented and analyzed in layers II/III of the mouse frontal cortex, in mice that slept, were spontaneously awake, or were acutely or chronically deprived of sleep (Fig. 1*A*; three mice per group; number of ROIs: S, 295; W, 266; SD, 355; CSR, 280). The amount of analyzed neuropil was similar across conditions [$>1\ mm^3$; Kruskal–Wallis (KW) test, $p = 0.45$; Fig. 1*B*]. The four groups also did not differ in analyzed astrocytic volume (KW test, $p = 0.11$, data not shown), nor in mean synaptic density per ROI (number of synapses/ROIs: S, 2.81; W, 3.03; SD, 2.93; CSR, 2.74). PAPs were easily recognized because of their morphological features (see Materials and Methods), and inside PAPs, AP was identified structurally by the presence of a portion of spine head, axon, or dendrite surrounded by the PAP, with a clear continuity between the part being enclosed by the PAP (phagosome) and the neuronal structure (see Fig. 1*C* for an example). Cumulative distribution analysis of all listed ROIs (S: $n = 289$; W: $n = 266$; SD: $n = 355$; CSR: $n = 280$) showed that in all mice AP affected only a small minority of synapses, but it changed across the experimental conditions (KW test, $p < 0.0001$). Specifically, AP occurred more frequently in CSR and SD mice than in S mice (percentage of all synapses within the ROI: CSR, 13.5%; W, 7.3%; SD, 8.4%; S, 5.7%; Dunn's multiple comparison test, CSR vs S, $p < 0.0001$; SD vs S, $p = 0.0076$; CSR vs SD, $p = 0.026$; Fig. 1*D*). In addition, we found that AP occurrence in W mice was comparable to S mice (Dunn's multiple comparison test, $p = 0.12$) and significantly different from CSR mice (Dunn's multiple comparison test, $p = 0.005$) but not from SD mice (Dunn's multiple comparison test, $p = 0.9$; Fig. 1*D*), suggesting that the increase in AP was related to sleep loss and not just to the wake state. Note that the increase in AP after sleep loss is unlikely to be explained by the exposure to novel objects and running wheels during acute and chronic sleep deprivation, because S and W mice were also exposed to the same stimuli during the dark phase. Further analysis of the specific structures of neuropil involved in AP revealed that axons and axonal boutons accounted for ~75% of all phagocyted elements, and spine heads for ~18–20% of all phagocyted elements (Fig. 1*D*). Components that could not be identified were rare, and parts of the dendritic shafts were almost never seen (Fig. 1*D*). Despite the change in absolute number of synapses involved in AP (AP+ synapses), the proportion of axons plus boutons relative to spine heads was primarily maintained across the four conditions (S, W, SD, CSR), suggesting that sleep loss promotes AP as a whole, with no specific effects on select components of the neuropil.

During early development, AP mediates the elimination of weak synapses in the lateral geniculate nucleus (Chung et al., 2013). Given the correlation between synaptic strength and size (Holtmaat and Svoboda, 2009), we measured the size of AP+ synapses to test whether small synapses were more frequently phagocyted by PAPs. We considered all synapses whose axon bouton or spine head was being phagocyted and measured their ASI, a reliable measure of synaptic strength that is also highly correlated with spine head volume (Desmond and Levy, 1988). AP involving other components outside the synapse (axons, dendrites, and unknown) was not considered in this analysis. We found that in all groups, the ASI of AP+ synapses was larger than the average ASI size [Mann–Whitney *U* (MW) test, $p < 0.01$] calculated from a pool of synapses randomly chosen in the S ($n = 302$ synapses), W ($n = 256$), SD ($n = 345$), and CSR ($n = 296$) datasets. Thus, independent of behavioral state, large synapses were more likely to show AP than synapses of medium or small size. We also quantified the prevalence of axonal boutons containing one or more mitochondria in AP+ and AP− synapses of comparable size (mitochondria are rare in spine heads; Sorra and Harris, 2000). As before, AP− synapses were selected from a pool of synapses randomly chosen from the S ($n = 216$ synapses), W ($n = 206$), SD ($n = 301$), and CSR ($n = 203$) datasets. In S and SD mice, a strong trend toward an increase in the number of axonal boutons with mitochondria was seen in AP+ synapses relative to AP− synapses (AP+ vs AP−: S, 57.2% vs 36.6%; SD, 50% vs 39.2%). However, Fisher's exact test did not reach significance (S, $p = 0.098$; SD, $p = 0.22$), and no changes were observed in the W (AP+ vs AP−: W, 45.7% vs 43.7%; $p = 0.86$) and CSR (AP+ vs AP−: 38.3% vs 40.9%; $p = 0.87$; Fig. 1*G*) groups.

In ~30% of ROIs, PAPs contained endosomes, defined as cytoplasmic membranous organelles of various size. To verify whether their number was affected by experimental condition, we annotated their presence while assessing AP. Since it was very difficult to visually distinguish endosomes based on the different types of inclusions, such as undigested engulfed synaptic material or partially digested material, we considered all endosomes containing some material as FE (Fig. 1*H*, left), whereas endosomes with no material were scored as EE (Fig. 1*H*, right). Notably, often EE appeared to form a complex tubular structure within the PAP in the 3D reconstruction (Fig. 1*I*). Although the number of FE did not change significantly across experimental conditions (KW test, $p = 0.13$), the number of EE showed a large increase in S mice relative to SD (MW test, $p < 0.0001$) and CSR (MW test, $p < 0.0001$) mice. The density of EE in W mice was different from S mice (MW test, $p = 0.045$) but also from SD (MW test, $p = 0.006$) and CSR (MW test, $p = 0.0002$) mice (Fig. 1*J*).

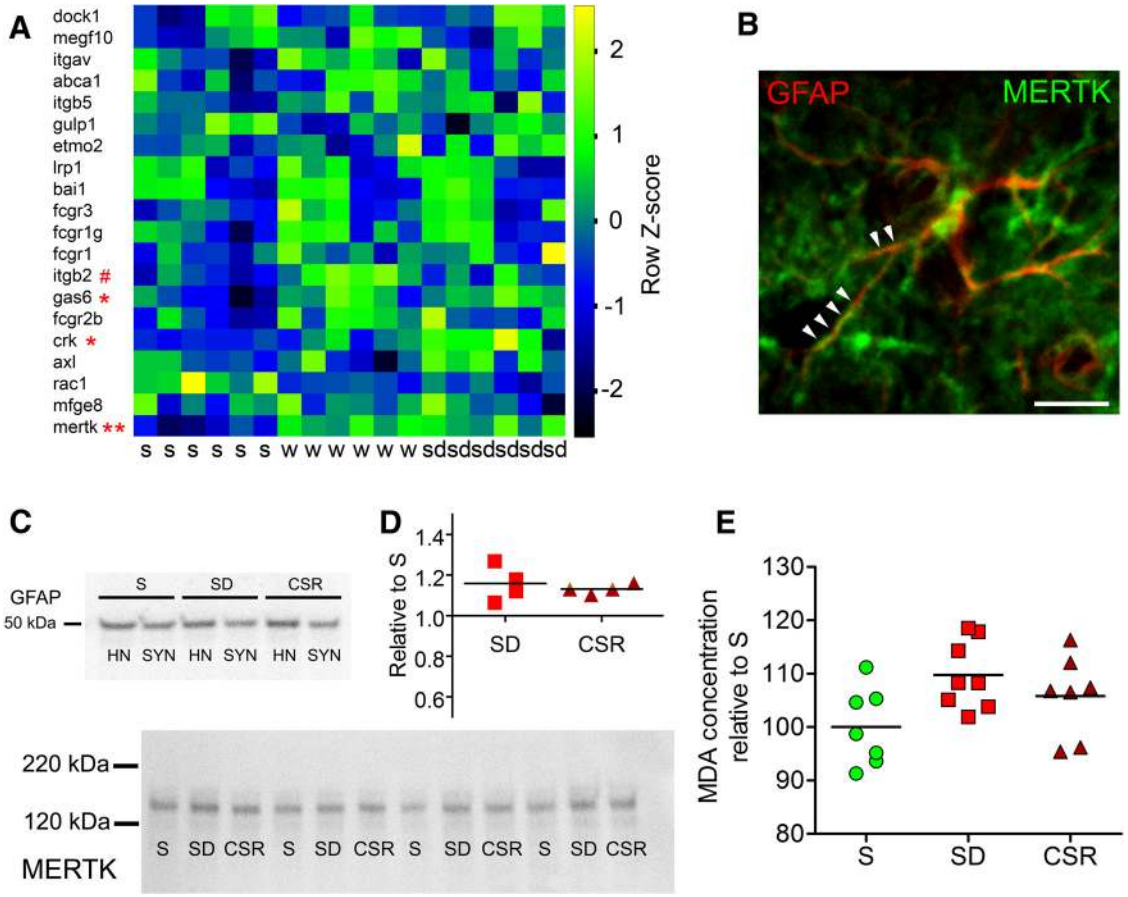

Figure 2. Sleep loss is associated with MERTK upregulation. ***A***, Heat diagram showing the expression levels of astrocytic genes previously identified (Cahoy et al., 2008) as indicative of phagocytosis in astrocytic-enriched samples of S, W, and SD adult heterozygous Aldh1L1-eGFP-L10a mice (Bellesi et al., 2015). $^{\#}p < 0.05$ in S versus W; $^{*}p < 0.1$ and $^{**}p < 0.01$ in S versus SD. ***B***, Example of an astrocyte stained with GFAP (red) and coexpressing MERTK (green) along its processes (arrowheads). Scale bar, 30 μm. ***C***, Top, GFAP expression in cortical homogenates (HN) and synaptoneurosomes (SYN). Bottom, Representative bands from S, SD, and CSR pools ($n = 4$ per pool) showing MERTK expression in cortical synaptoneurosomes. ***D***, Western blot quantification of MERTK expression in SD ($p < 0.05$) and CSR ($p < 0.05$) relative to S. ***E***, Lipid peroxidation analysis showing MDA concentration for S, SD, and CSR mice (KW test, $p = 0.065$).

Sleep loss increases the expression of MERTK

In a recent study in Aldh1L1-eGFP-L10a mice, we used translating ribosome affinity purification technology and microarrays to identify astrocytic genes whose expression is affected by the sleep/wake cycle and found *Mertk* among the "wake" genes, upregulated in both spontaneous wake and acute sleep deprivation relative to sleep (Bellesi et al., 2015). Here the same data sets (NCBI GEO accession number GSE69079) were interrogated by comparing S either with forced wake or with spontaneous wake, to determine whether among the previously identified astrocytic transcripts involved in phagocytosis (Cahoy et al., 2008) some were specifically affected by acute sleep loss but not by spontaneous wake. We found little evidence for additional activation of phagocytic genes in forced wake relative to spontaneous wake: *Mertk* showed a similar increase in both comparisons (S vs W, $p = 0.005$; S vs SD, $p = 0.003$; Fig. 2*A*), and *Gas6*, the MERTK ligand, also showed a similar trend toward an increase (both $p = 0.06$; Fig. 2*A*). The only difference was *crk*, whose protein interacts with DOCK1, the downstream pathway of MERTK, which trended to increase ($p = 0.06$) only after forced wake, and *Itgb2*, which instead increased ($p = 0.014$) only after spontaneous wake (Fig. 2*A*). Overall, these results suggest that a few hours of wake are sufficient to activate the MERTK pathway, even without sleep loss. To verify whether *Mertk* was upregulated also at the protein level, we first double stained coronal sections of frontal cortex with antibodies against MERTK and GFAP, a well recognized marker for astrocytes. We confirmed that several astrocytic processes were MERTK positive (Fig. 2*B*), as described previously (Chung et al., 2013). Then, to assess the MERTK expression level in nearby synapses, we prepared cortical synaptoneurosomes from S, SD, and CSR mice, and after checking that synaptoneurosomes still contained perisynaptic glia using the astrocytic marker GFAP (Fig. 2*C*, top), we measured MERTK protein expression (Fig. 2*C*, bottom). Quantitative immunoblot analysis showed that both SD (Dunn's multiple comparison test, $p < 0.05$) and CSR (Dunn's multiple comparison test, $p < 0.05$) were associated with higher MERTK levels relative to S, and the increase was similar in the two conditions (Fig. 2*D*), again suggesting that the activation of MERTK is linked to being awake but does not reflect the severity and/or duration of sleep loss.

Through the action of Gas6, the MERTK receptor can recognize "eat-me" signals on the membrane of the cell that needs to be phagocyted. These signals include the exposure of phosphatidylserine on the outer leaflet of the plasma membrane (Ravichandran, 2010), which can occur because of oxidative stress (Kagan et al., 2002; Brown and Neher, 2014). To assess whether sleep loss was associated with high levels of oxidative stress at the synaptic level, we measured the extent of lipid peroxidation by quantifying free MDA, a lipid peroxidation end product, in cortical synaptoneurosomes of S, SD, and CSR mice. Colorimetric quantification of MDA levels showed a similar trend toward an increase in SD and CSR mice relative to S mice (KW test, $p = 0.065$), whereas

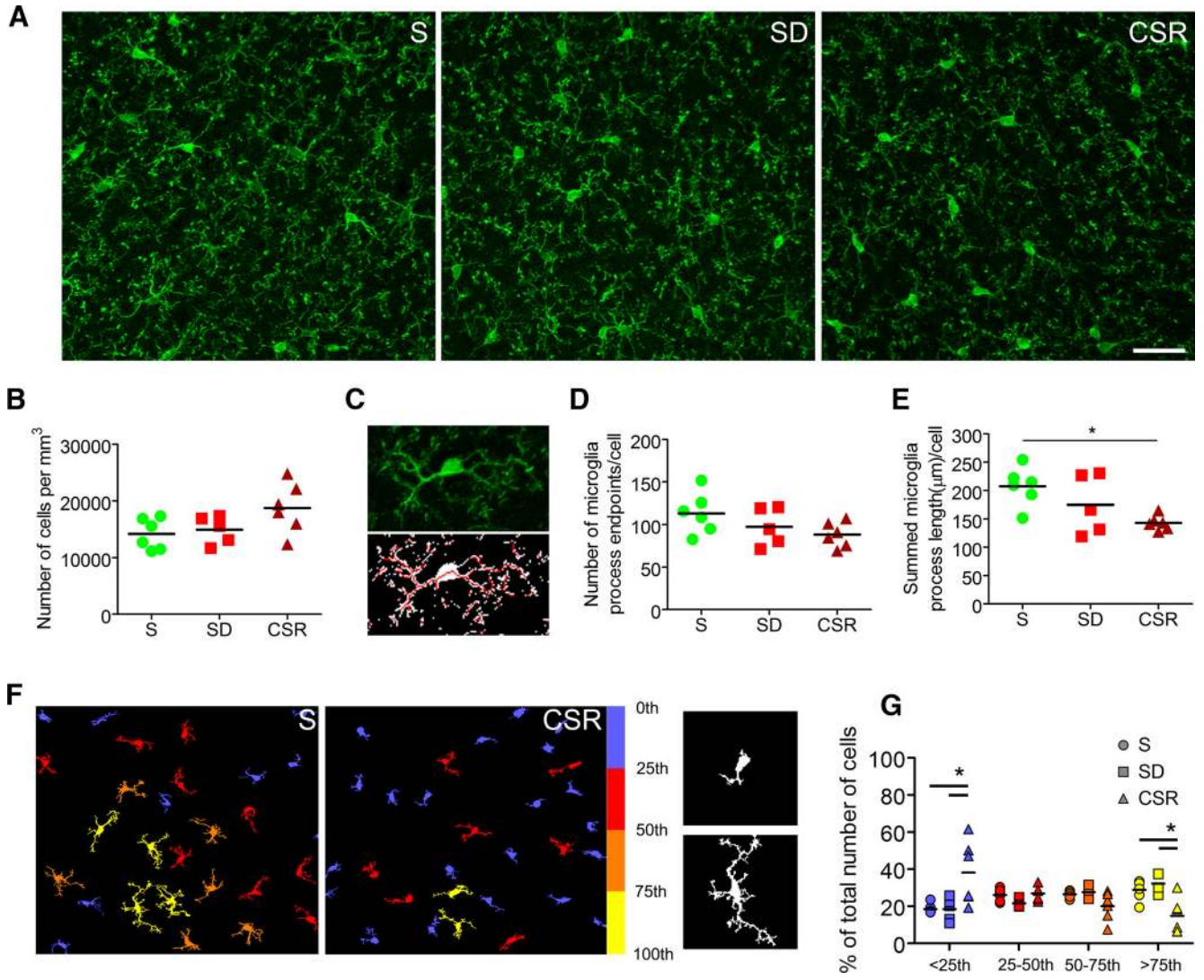

Figure 3. Chronic sleep loss is associated with microglia activation. ***A***, Raw images from S ($n = 6$), SD ($n = 5$), and CSR ($n = 6$) mice (frontal cortex) showing IBA-1 staining. Scale bar, 30 μm. ***B***, Number of IBA-1-positive cells per cubed millimeter in S, SD, and CSR mice. ***C***, Example of one IBA-1-positive microglial cell as it appears from the raw image and after processing (despeckling and skeletonizing). ***D***, ***E***, Number of end points per cell (***D***) and sum of all process lengths per microglial cell (***E***) in S, SD, and CSR mice. *$p < 0.05$. ***F***, Left, Examples from S and CSR fields showing processed and color-coded IBA-1 microglial cells (yellow, more ramified; blue, less ramified). Right, Examples of poorly ramified (above) and very ramified (below) IBA-1 microglial cells. ***G***, Distribution in quartiles of the number of IBA-1 microglial cells ranked by area size, an indirect measure of the complexity of process branching. *$p < 0.05$.

no difference was observed between SD and CSR (MW test, $p = 0.4$; Fig. 2*E*).

Chronic sleep restriction is associated with microglia activation

MERTK protein is also expressed in microglia (Chung et al., 2013), and microglia contributes to synaptic elimination during normal development (Paolicelli et al., 2011; Schafer et al., 2012; Bialas and Stevens, 2013) and in response to monocular deprivation (Sipe et al., 2016). Thus, we sought to assess whether sleep loss leads to microglia activation in mouse cerebral cortex. We stained S, SD, and CSR brain sections with IBA-1, a recognized marker for microglia and quantified microglia density in the frontal cortex (Fig. 3*A*). Despite a small increase in CSR relative to SD and S mice, we found no significant changes in cell number (KW test, $p = 0.09$; Fig. 3*B*). Then, we analyzed the morphology of microglial cells, since it correlates closely with their state of activation (Kreutzberg, 1996; Nimmerjahn et al., 2005). To quantify the complexity of microglia branching, we used two different validated approaches. The first method (Morrison and Filosa, 2013) calculates the number of process end points per cell and the length of microglia processes per cell by skeletonizing despeckled IBA-1-stained fields (Fig. 3*C*). The number of end points per cell did not significantly change across conditions (KW test, $p = 0.15$), although a trend toward a decrease was present in CSR relative to S animals (MW test, $p = 0.06$; Fig. 3*D*). Pairwise comparisons between groups (S vs SD, SD vs CSR) were not significant. Quantitative analysis showed instead a significant reduction of process length per cell in CSR relative to S mice (MW test, $p = 0.004$; Fig. 3*E*). In the second approach, using a custom-made Matlab algorithm based on the study by Kozlowski and Weimer (2012), we measured the area and perimeter of automatically, individually identified IBA-1 microglial cells. For each experimental group, cells were clustered in quartiles (from small area/perimeter to large area/perimeter), and the relative number of cells within each quartile was estimated (Fig. 3*F*). Repeated-measures two-way ANOVA with experimental group as the between factor and quartiles as the within factor showed a main effect of experimen-

tal group (area: $F_{(2,14)} = 4.16$, $p = 0.038$; perimeter: $F_{(2,14)} = 3.74$, $p = 0.05$) and a significant interaction (area: $F_{(6,42)} = 6.82$, $p < 0.001$; perimeter: $F_{(6,42)} = 6.35$, $p < 0.001$). *Post hoc* analysis found that in the first quartile, the number of cells was higher in CSR mice relative to S (area: Bonferroni's test, $t = 4.78$; $p < 0.001$; perimeter: Bonferroni's test, $t = 4.95$; $p < 0.001$) and SD (area: Bonferroni's test, $t = 4.58$; $p < 0.001$; perimeter: Bonferroni's test, $t = 4.68$; $p < 0.001$) mice, whereas the opposite was true in the fourth quartile (CSR vs S, area: Bonferroni's test, $t = 3.44$, $p < 0.01$; perimeter: Bonferroni's test, $t = 3.44$, $p < 0.01$; CSR vs SD, area: Bonferroni's test, $t = 4.06$, $p < 0.001$; perimeter: Bonferroni's test, $t = 3.44$, $p < 0.01$). These results suggest that there was a higher number of less ramified cells and a lower number of well ramified cells in CSR mice relative to SD and S mice (Fig. 3*G*, values for perimeter are not shown).

Furthermore, we investigated whether sleep loss promoted microglial phagocytosis by quantifying the number and volume of presynaptic terminals, identified as VGLUT-1-positive puncta with confocal microscopy, which were engulfed within IBA-1-stained cells. Only VGLUT-1-positive puncta larger than 100 pixels (roughly corresponding to 0.03 μm^3) and showing an overlap of 100% in *xyz* with microglial cells were considered as phagocyted (Fig. 4*A–C*). Quantitative analysis showed that the number and volume of phagocyted VGLUT-1 puncta changed significantly across conditions (KW test; number, $p = 0.03$; volume, $p = 0.03$). Specifically, phagocyted VGLUT-1 puncta were more numerous in CSR mice than S mice (density, $+27.98 \pm 13.56\%$; MW test, $p = 0.009$) and larger in CSR mice than S mice ($+32.13 \pm 22.38\%$; MW test, $p = 0.026$) and SD mice ($+38.52 \pm 23.46\%$; MW test, $p = 0.03$; Fig. 4*D*,*E*). The percentage of VGLUT-1 puncta engulfed within microglia relative to the total number of VGLUT-1 puncta was higher in CSR mice ($0.39 \pm 0.14\%$) than S ($0.22 \pm 0.07\%$; MW test, $p = 0.04$) and SD ($0.19 \pm 0.06\%$, MW test, $p = 0.017$; data not shown) mice.

To further characterize microglial-mediated phagocytosis, we measured C3 expression levels in cortical homogenates of S, SD, and CSR mice. C3, a central component of the complement cascade, is deposited on cell debris and can directly activate C3 receptors on microglia, thus triggering phagocytosis. Western blot analysis showed that C3 expression was higher in CSR mice than S mice (Dunn's multiple comparison test, $p = 0.04$). Despite some variability, SD mice also showed higher C3 levels than S animals (Dunn's multiple comparison test, $p = 0.04$), suggesting that even shorter periods of sleep loss can trigger C3 activation (Fig. 4*F*). Overall, these results indicate that CSR is associated with microglia activation and increased phagocytosis.

Finally, we ascertained whether microglia activation was associated with increased levels of inflammatory mediators in the CSF. CSF was extracted in additional groups of S, SD, and CSR mice. Multiplex immune assay analysis showed that 14 of the 23 molecules analyzed (i.e., IL1a, IL2, IL3, IL4, IL5, IL6, IL10, IL12, IL17a, G-CSF, IFNγ, MIP1a, and RANTES) were undetectable in almost all CSF samples. Nine of the remaining molecules (i.e., IL1b, IL9, IL12, IL13, Eotaxin, KC, MCP1, MIP1b, and TNFα) were detected in 34–100% of samples. Levels of IL1b, IL9, IL12, IL13, Eotaxin, KC, MCP1, and MIP1b did not change significantly across groups, whereas levels of TNFα were higher in S mice relative to SD (MW test, $p = 0.018$) and CSR (MW test, $p = 0.047$; Fig. 4*G*). Overall, these results indicate that CSR is associated with microglia activation and increased phagocytosis without a notable increase of inflammatory mediators in the CSF.

Discussion

We show that acute sleep deprivation and chronic sleep loss increase the number of phagocytic events mediated by astrocytes in the mouse cortical neuropil, whereas only chronic sleep loss can trigger microglial phagocytosis. In astrocytes, phagocytosis is associated with increased MERTK expression and lipid peroxidation, whereas microglial phagocytosis is associated with increased levels of the complement component C3 without clear signs of inflammations in CSF.

Only a few synapses are affected by AP: peripheral astrocytic processes target 80% of all excitatory synapses, the larger ones, and <10% of them on average undergo AP. Our adolescent mice had already experienced the critical period of most intense synaptic pruning, but more subtle synaptic refinement was likely still occurring (Hoel et al., 2016). Early developmental phagocytosis mainly targets presynaptic elements of transient, likely weaker, retinogeniculate synapses (Schafer et al., 2012; Chung et al., 2013). By contrast, wake-enhanced phagocytosis preferentially targets larger, and thus stronger, synapses and often involves axonal elements outside the presynaptic terminal. Thus, glial phagocytosis may serve different functions: elimination of exuberant synapses during early development and degradation of components of strong, likely well established synapses in response to extended wake during adolescence. Astrocytes could promote the housekeeping of worn synaptic components, especially axonal elements, by degrading portions of their membranes, perhaps damaged by excessive lipid peroxidation. Of note, we found that the presence of mitochondria within the presynaptic boutons did not increase the likelihood of a synapse to be phagocyted. At first, this result seems to exclude a direct link between oxidative energy metabolism and AP. However, mitochondria are present in only ~40% of presynaptic terminals (Chavan et al., 2015; de Vivo et al., 2017) and are rarely seen in spine heads (Sorra and Harris, 2000), which are characterized by intense metabolic activity (Harris et al., 2012), suggesting that the presence of mitochondria may be a poor marker of the overall metabolic activity of a synapse.

Our results suggest that extended wake enhances AP through a mechanism that involves the MERTK receptor. In fact, a few hours of spontaneous wake are sufficient to upregulate *Merkt* expression relative to sleep (Bellesi et al., 2015), but not to increase the incidence of AP (this study). Thus, the activation of the MERTK pathway may start during spontaneous wake, but its long-term, structural consequences become apparent only after sustained sleep loss. MERTK recognizes "eat me signals" presented in target debris (Ravichandran, 2010). One of them is phosphatidylserine, a phospholipid normally confined to the inner leaflet of the plasma membrane, which triggers phagocytosis when exposed on the cell surface. Increased calcium concentrations, ATP depletion, and oxidative stress are all factors linked to cell activity and metabolism that can induce membrane translocation of phosphatidylserine (Brown and Neher, 2014). Since synaptic activity accounts for most of the brain's energy budget (Harris et al., 2012), greater metabolic activity and/or increased production of waste induced by extended wake (Cirelli et al., 2006) could favor the externalization of phosphatidylserine on the plasma membrane of heavily used synapses. Another possible mechanism involves C1q, which localizes at the sites of synaptic elimination in the developing reticulogeniculate system (Stevens et al., 2007). The expression of all three subunits of the C1q complex is upregulated when retinal ganglion cells are exposed to astrocytes, and through C3 activation, C1q can initiate synapse elimination by the classical complement cascade (Stevens et al.,

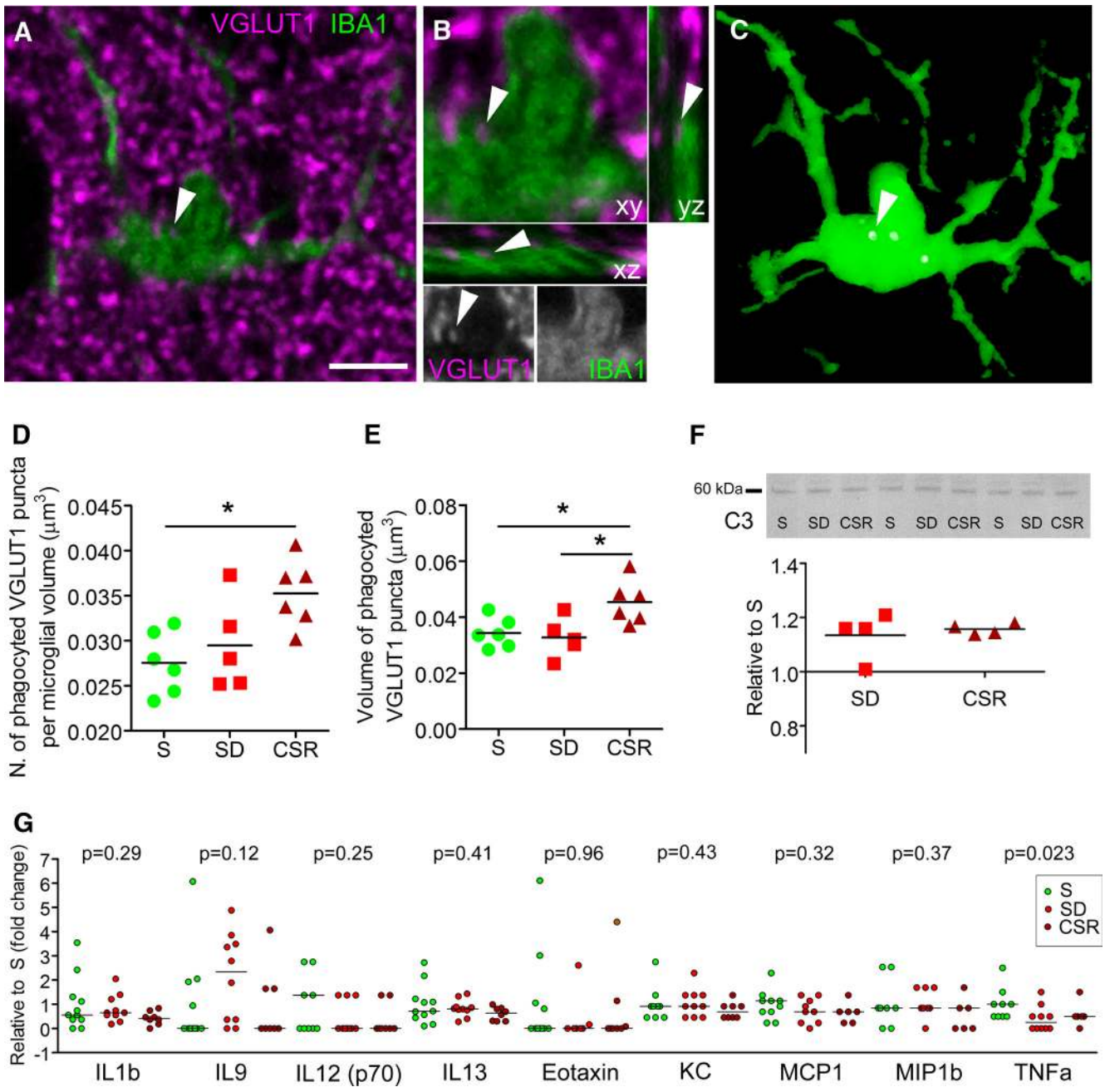

Figure 4. Chronic sleep loss is associated with microglial phagocytosis. ***A***, Raw image showing an IBA-1-positive microglia (green) and VGLUT-1 puncta staining (magenta) in a representative CSR mouse. Scale bar, 5 μm. ***B***, Enlarged frame of the cell shown in ***A***, visualized also in the *xz* and *yz* projections and in gray separated channels, showing a VGLUT-1-positive element engulfed within the microglial soma (arrowheads). ***C***, 3D reconstruction of the same cell showing the engulfed VGLUT-1 element (arrowhead). ***D***, ***E***, Number (***D***) and volume (***E***) of phagocyted VGLUT-1 elements per microglial cell for S ($n = 6$), SD ($n = 5$), and CSR ($n = 6$). *$p < 0.05$. ***F***, Western blot analysis of the complement component C3 for SD and CSR pools relative to S pools. Representative bands are depicted above from cortical homogenates of S, SD, and CSR pools ($n = 4$ per pool). ***G***, Protein levels of cytokines and chemokines in CSF from S ($n = 11$), SD ($n = 10$), and CSR ($n = 8$) mice. Protein levels were measured in individual CSF specimens using multiplex magnetic bead technology for the simultaneous measurement of the 23 cytokines/chemokines. Shown is the expression of the detected molecules and the relative *p* values obtained from the KW test.

2007). Of note, the C1q subunit β mRNA is upregulated in the cortex of adult rats in wake relative to sleep (Cirelli et al., 2004), and in the current study, C3 levels increased after acute and chronic sleep loss relative to sleep. Using the same dataset of this study, we recently also found that synaptic density in frontal cortex does not change between S and SD, and most spines decrease in size during sleep in a manner proportional to their size (de Vivo et al., 2017). Crucially, this downscaling is diffuse but selective, sparing the large synapses (de Vivo et al., 2017) in which we show here that AP is more common. Thus, stronger and more "rigid" synapses, whose strength does not seem to change between sleep and wake, may use AP to recycle structural components and guarantee a proper synaptic function, perhaps not only in response to damage, but to prevent it.

In addition to AP, we also found endosomes enclosed within the PAPs. In eukaryotic cells, endosomes are involved in membrane recycling, receptor trafficking, exocytosis, and cellular waste disposal (Maxfield and McGraw, 2004). In PAPs, we cannot exclude that some of the endosomes, those containing undigested material resembling presynaptic vesicles, represent further

steps of the phagocytosis process. On the other hand, the reduction of empty endosomes after chronic sleep loss may indicate that they are being used during the engulfment process and/or to recycle heavily used portions of cytoplasmic membrane. Independent of its functional significance, which is still unclear, this finding is in line with the results of a recent study that characterized ultrastructural changes in the cell body of cortical pyramidal neurons and found that empty endosomes were more frequently observed in S relative to CSR mice (de Vivo et al., 2016).

Microglial cells, the resident innate immune cells in the brain, are alert sentinels of the nervous system clearing debris, looking for signs of infiltration by infectious agents, and mediating the inflammatory and repair response to several brain injuries (Nimmerjahn et al., 2005; Hanisch and Kettenmann, 2007; Tay et al., 2017). Microglia regularly extend their protrusions to briefly touch and sense the functional state of synapses in an activity-dependent manner (Wake et al., 2009; Tremblay et al., 2010), and their role in developmental synaptic pruning has recently been recognized (Paolicelli et al., 2011; Schafer et al., 2012; Bialas and Stevens, 2013; Sipe et al., 2016). The two molecular mechanisms discussed above as potential mediators of the wake-related activation of AP could also apply to microglia, which express both MERTK and C3 receptors (Stevens et al., 2007; Chung et al., 2013) and could be activated by some form of damage at synaptic membranes triggered by sustained neuronal activity. However, direct morphological evidence of microglial activation with transition to an active ameboid state, and signs of microglial phagocytosis, were only found after chronic sleep restriction, suggesting that severe and sustained sleep loss is required to fully engage microglia. Microglial and astrocytic activation were reported in the rat hippocampus after 5 d of total sleep deprivation (Hsu et al., 2003). Moreover, mice treated with the antibiotic minocycline, an inhibitor of microglial activation, showed a reduced rebound in slow-wave activity after 3 h of sleep deprivation, prompting the authors to suggest that microglial activation may contribute to the buildup of sleep need during extended wake (Wisor et al., 2011). In the same study, however, short sleep deprivation did not increase the expression of IL1β, IL6, and TNFα in brain homogenates and decreased the expression of CD11b, which is enriched in microglia (Wisor et al., 2011). We found that 6–8 h of sleep deprivation, which consistently trigger a sleep rebound with increased slow-wave activity (Bellesi et al., 2015), did not lead to microglial activation. Thus, in our experimental conditions, microglia are unlikely to play a role in sleep homeostasis.

Microglial activation after chronic sleep loss occurred without signs of neuroinflammation. In both animals and humans, sleep loss has been associated with a pro-inflammatory state (Mullington et al., 2010; Hurtado-Alvarado et al., 2013), and perhaps our CSF assay was not sensitive enough to detect mild inflammation. Alternatively, CSF inflammation may occur only in fully blown pathological states but not in response to sleep loss per se. Since microglia, like astrocytes, participate in the removal of synaptic debris, their activation during prolonged wake may represent the physiological response of these cells to worn synapses. An alternative explanation, however, is suggested by the finding that sleep promotes the clearance of amyloid-β from the interstitial space (Xie et al., 2013) whereas sleep deprivation promotes the deposition of amyloid plaques (Lim et al., 2014), which in turn can lead to microglia activation (Xiang et al., 2006; Halle et al., 2008; Jung et al., 2015). Persistent microglial activation, even at a low level (microglia priming), can lead to exaggerated and detrimental responses to a secondary insult, further promoting pathological states (Perry and Holmes, 2014). Thus, we speculate that by priming microglia, chronic sleep loss may increase the brain's susceptibility to other forms of damage, including neurodegeneration (Perry and Holmes, 2014; Calcia et al., 2016), although this idea needs to be tested directly.

Our molecular screening identified *Mertk* and *crk* transcripts, both belonging to the MERTK pathway, as the only astrocytic genes linked to phagocytosis and overexpressed after sleep deprivation relative to sleep (Bellesi et al., 2015). Yet, the current study is correlational, and we do not know whether MERTK and C3 receptors are necessary or sufficient for sleep loss-mediated phagocytosis. Future experiments may be able to causally link the astrocytic and microglial molecular changes to sleep loss, for instance by using *Mertk*−/− (Chung et al., 2013) and *CR3*−/− (Schafer et al., 2012) mice.

References

Bellesi M, Vyazovskiy VV, Tononi G, Cirelli C, Conti F (2012) Reduction of EEG theta power and changes in motor activity in rats treated with ceftriaxone. PloS One 7:e34139. CrossRef Medline

Bellesi M, Pfister-Genskow M, Maret S, Keles S, Tononi G, Cirelli C (2013) Effects of sleep and wake on oligodendrocytes and their precursors. J Neurosci 33:14288–14300. CrossRef Medline

Bellesi M, de Vivo L, Tononi G, Cirelli C (2015) Effects of sleep and wake on astrocytes: clues from molecular and ultrastructural studies. BMC Biol 13:66. CrossRef Medline

Berbel P, Innocenti GM (1988) The development of the corpus callosum in cats: a light- and electron-microscopic study. J Comp Neurol 276:132–156. CrossRef Medline

Bialas AR, Stevens B (2013) TGF-beta signaling regulates neuronal C1q expression and developmental synaptic refinement. Nat Neurosci 16:1773–1782. CrossRef Medline

Brown GC, Neher JJ (2014) Microglial phagocytosis of live neurons. Nat Rev Neurosci 15:209–216. CrossRef Medline

Cahoy JD, Emery B, Kaushal A, Foo LC, Zamanian JL, Christopherson KS, Xing Y, Lubischer JL, Krieg PA, Krupenko SA, Thompson WJ, Barres BA (2008) A transcriptome database for astrocytes, neurons, and oligodendrocytes: a new resource for understanding brain development and function. J Neurosci 28:264–278. CrossRef Medline

Calcia MA, Bonsall DR, Bloomfield PS, Selvaraj S, Barichello T, Howes OD (2016) Stress and neuroinflammation: a systematic review of the effects of stress on microglia and the implications for mental illness. Psychopharmacology (Berl) 233:1637–1650. CrossRef

Chavan V, Willis J, Walker SK, Clark HR, Liu X, Fox MA, Srivastava S, Mukherjee K (2015) Central presynaptic terminals are enriched in ATP but the majority lack mitochondria. PloS One 10:e0125185. CrossRef Medline

Chung WS, Clarke LE, Wang GX, Stafford BK, Sher A, Chakraborty C, Joung J, Foo LC, Thompson A, Chen C, Smith SJ, Barres BA (2013) Astrocytes mediate synapse elimination through MEGF10 and MERTK pathways. Nature 504:394–400. CrossRef Medline

Chung WS, Allen NJ, Eroglu C (2015) Astrocytes control synapse formation, function, and elimination. Cold Spring Harb Perspect Biol 7:a020370. CrossRef Medline

Cirelli C, Gutierrez CM, Tononi G (2004) Extensive and divergent effects of sleep and wakefulness on brain gene expression. Neuron 41:35–43. CrossRef Medline

Cirelli C, Faraguna U, Tononi G (2006) Changes in brain gene expression after long-term sleep deprivation. J Neurochem 98:1632–1645. CrossRef

Davis CH, Kim KY, Bushong EA, Mills EA, Boassa D, Shih T, Kinebuchi M, Phan S, Zhou Y, Bihlmeyer NA, Nguyen JV, Jin Y, Ellisman MH, Marsh-Armstrong N (2014) Transcellular degradation of axonal mitochondria. Proc Natl Acad Sci U S A 111:9633–9638. CrossRef Medline

Desmond NL, Levy WB (1988) Synaptic interface surface area increases with long-term potentiation in the hippocampal dentate gyrus. Brain Res 453:308–314. CrossRef Medline

de Vivo L, Nelson AB, Bellesi M, Noguti J, Tononi G, Cirelli C (2016) Loss of sleep affects the ultrastructure of pyramidal neurons in the adolescent mouse frontal cortex. Sleep 39:861–874. CrossRef Medline

de Vivo L, Bellesi M, Marshall W, Bushong EA, Ellisman MH, Tononi G,

Cirelli C (2017) Ultrastructural evidence for synaptic scaling across the wake/sleep cycle. Science 355:507–510. CrossRef Medline

Everson CA (2005) Clinical assessment of blood leukocytes, serum cytokines, and serum immunoglobulins as responses to sleep deprivation in laboratory rats. Am J Physiol Regul Integr Comp Physiol 289:R1054–R1063. CrossRef Medline

Grommes C, Lee CY, Wilkinson BL, Jiang Q, Koenigsknecht-Talboo JL, Varnum B, Landreth GE (2008) Regulation of microglial phagocytosis and inflammatory gene expression by Gas6 acting on the Axl/Mer family of tyrosine kinases. J Neuroimmune Pharmacol 3:130–140. CrossRef Medline

Halle A, Hornung V, Petzold GC, Stewart CR, Monks BG, Reinheckel T, Fitzgerald KA, Latz E, Moore KJ, Golenbock DT (2008) The NALP3 inflammasome is involved in the innate immune response to amyloid-beta. Nat Immunol 9:857–865. CrossRef Medline

Hanisch UK, Kettenmann H (2007) Microglia: active sensor and versatile effector cells in the normal and pathologic brain. Nat Neurosci 10:1387–1394. CrossRef Medline

Harris JJ, Jolivet R, Attwell D (2012) Synaptic energy use and supply. Neuron 75:762–777. CrossRef Medline

He J, Hsuchou H, He Y, Kastin AJ, Wang Y, Pan W (2014) Sleep restriction impairs blood–brain barrier function. J Neurosci 34:14697–14706. CrossRef Medline

Hoel EP, Albantakis L, Cirelli C, Tononi G (2016) Synaptic refinement during development and its effect on slow-wave activity: a computational study. J Neurophysiol 115:2199–2213. CrossRef Medline

Holtmaat A, Svoboda K (2009) Experience-dependent structural synaptic plasticity in the mammalian brain. Nat Rev Neurosci 10:647–658. CrossRef Medline

Hsu JC, Lee YS, Chang CN, Chuang HL, Ling EA, Lan CT (2003) Sleep deprivation inhibits expression of NADPH-d and NOS while activating microglia and astroglia in the rat hippocampus. Cells Tissues Organs 173:242–254. CrossRef Medline

Hurtado-Alvarado G, Pavón L, Castillo-García SA, Hernández ME, Domínguez-Salazar E, Velázquez-Moctezuma J, Gómez-González B (2013) Sleep loss as a factor to induce cellular and molecular inflammatory variations. Clin Dev Immunol 2013:801341. Medline

Jung CK, Keppler K, Steinbach S, Blazquez-Llorca L, Herms J (2015) Fibrillar amyloid plaque formation precedes microglial activation. PloS One 10:e0119768. CrossRef Medline

Kagan VE, Gleiss B, Tyurina YY, Tyurin VA, Elenstrom-Magnusson C, Liu SX, Serinkan FB, Arroyo A, Chandra J, Orrenius S, Fadeel B (2002) A role for oxidative stress in apoptosis: oxidation and externalization of phosphatidylserine is required for macrophage clearance of cells undergoing Fas-mediated apoptosis. J Immunol 169:487–499. CrossRef Medline

Kozlowski C, Weimer RM (2012) An automated method to quantify microglia morphology and application to monitor activation state longitudinally in vivo. PloS One 7:e31814. CrossRef Medline

Kreutzberg GW (1996) Microglia: a sensor for pathological events in the CNS. Trends Neurosci 19:312–318. CrossRef Medline

Lim MM, Gerstner JR, Holtzman DM (2014) The sleep-wake cycle and Alzheimer's disease: what do we know? Neurodegener Dis Manag 4:351–362. CrossRef Medline

Maret S, Faraguna U, Nelson AB, Cirelli C, Tononi G (2011) Sleep and waking modulate spine turnover in the adolescent mouse cortex. Nat Neurosci 14:1418–1420. CrossRef Medline

Maxfield FR, McGraw TE (2004) Endocytic recycling. Nat Rev Mol Cell Biol 5:121–132. CrossRef Medline

Morrison HW, Filosa JA (2013) A quantitative spatiotemporal analysis of microglia morphology during ischemic stroke and reperfusion. J Neuroinflammation 10:4. CrossRef Medline

Mullington JM, Simpson NS, Meier-Ewert HK, Haack M (2010) Sleep loss and inflammation. Best Pract Res Clin Endocrinol Metab 24:775–784. CrossRef Medline

Nguyen JV, Soto I, Kim KY, Bushong EA, Oglesby E, Valiente-Soriano FJ, Yang Z, Davis CH, Bedont JL, Son JL, Wei JO, Buchman VL, Zack DJ, Vidal-Sanz M, Ellisman MH, Marsh-Armstrong N (2011) Myelination transition zone astrocytes are constitutively phagocytic and have synuclein dependent reactivity in glaucoma. Proc Natl Acad Sci U S A 108:1176–1181. CrossRef Medline

Nimmerjahn A, Kirchhoff F, Helmchen F (2005) Resting microglial cells are highly dynamic surveillants of brain parenchyma in vivo. Science 308:1314–1318. CrossRef Medline

Paolicelli RC, Bolasco G, Pagani F, Maggi L, Scianni M, Panzanelli P, Giustetto M, Ferreira TA, Guiducci E, Dumas L, Ragozzino D, Gross CT (2011) Synaptic pruning by microglia is necessary for normal brain development. Science 333:1456–1458. CrossRef Medline

Perry VH, Holmes C (2014) Microglial priming in neurodegenerative disease. Nat Rev Neurol 10:217–224. CrossRef Medline

Ravichandran KS (2010) Find-me and eat-me signals in apoptotic cell clearance: progress and conundrums. J Exp Med 207:1807–1817. CrossRef Medline

Schafer DP, Lehrman EK, Kautzman AG, Koyama R, Mardinly AR, Yamasaki R, Ransohoff RM, Greenberg ME, Barres BA, Stevens B (2012) Microglia sculpt postnatal neural circuits in an activity and complement-dependent manner. Neuron 74:691–705. CrossRef Medline

Schindelin J, Arganda-Carreras I, Frise E, Kaynig V, Longair M, Pietzsch T, Preibisch S, Rueden C, Saalfeld S, Schmid B, Tinevez JY, White DJ, Hartenstein V, Eliceiri K, Tomancak P, Cardona A (2012) Fiji: an open-source platform for biological-image analysis. Nat Methods 9:676–682. CrossRef Medline

Sipe GO, Lowery RL, Tremblay MÈ, Kelly EA, Lamantia CE, Majewska AK (2016) Microglial P2Y12 is necessary for synaptic plasticity in mouse visual cortex. Nat Commun 7:10905. CrossRef Medline

Sorra KE, Harris KM (2000) Overview on the structure, composition, function, development, and plasticity of hippocampal dendritic spines. Hippocampus 10:501–511. CrossRef Medline

Stevens B, Allen NJ, Vazquez LE, Howell GR, Christopherson KS, Nouri N, Micheva KD, Mehalow AK, Huberman AD, Stafford B, Sher A, Litke AM, Lambris JD, Smith SJ, John SW, Barres BA (2007) The classical complement cascade mediates CNS synapse elimination. Cell 131:1164–1178. CrossRef Medline

Tay TL, Savage JC, Hui CW, Bisht K, Tremblay MÈ (2017) Microglia across the lifespan: from origin to function in brain development, plasticity and cognition. J Physiol 595:1929–1945. CrossRef Medline

Tremblay MÈ, Lowery RL, Majewska AK (2010) Microglial interactions with synapses are modulated by visual experience. PLoS Biol 8:e1000527. CrossRef Medline

Wake H, Moorhouse AJ, Jinno S, Kohsaka S, Nabekura J (2009) Resting microglia directly monitor the functional state of synapses *in vivo* and determine the fate of ischemic terminals. J Neurosci 29:3974–3980. CrossRef Medline

Wisor JP, Schmidt MA, Clegern WC (2011) Evidence for neuroinflammatory and microglial changes in the cerebral response to sleep loss. Sleep 34:261–272. CrossRef Medline

Xiang Z, Haroutunian V, Ho L, Purohit D, Pasinetti GM (2006) Microglia activation in the brain as inflammatory biomarker of Alzheimer's disease neuropathology and clinical dementia. Dis Markers 22:95–102. CrossRef Medline

Xie L, Kang H, Xu Q, Chen MJ, Liao Y, Thiyagarajan M, O'Donnell J, Christensen DJ, Nicholson C, Iliff JJ, Takano T, Deane R, Nedergaard M (2013) Sleep drives metabolite clearance from the adult brain. Science 342:373–377. CrossRef Medline